nature communications

Article

https://doi.org/10.1038/s41467-025-56483-9

Single soliton microcomb combined with optical phased array for parallel FMCW LiDAR

Received: 8 June 2024

Accepted: 14 January 2025

Published online: 26 January 2025

Check for updates

Jingye Chen[1,4], Wenlei Li[1,4], Zhe Kang[1,2,4], Zongxing Lin[1], Shi Zhao[1], Daixin Lian[1], Jijun He[2], Dongmei Huang[3], Daoxin Dai[1] & Yaocheng Shi[1]

The frequency-modulated continuous-wave (FMCW) technology combined with optical phased array (OPA) is promising for the all-solid-state light detection and ranging (LiDAR). We propose and experimentally demonstrate a silicon integrated OPA combined with an optical frequency microcomb for parallel LiDAR system. For realizing the parallel wavelengths emission consistent with Rayleigh criterion, the wide waveguide beyond single mode region combined with the bound state in the continuum (BIC) effect is harnessed to obtain an ultra-long optical grating antenna array. The single soliton comb, generating about multiple distinct wavelength channels and combined with the high performance integrated OPA, is also demonstrated for coherent three-dimensional (3D) imaging by utilizing FMCW method. The modulation bandwidth of parallel modulation of the microcomb is beyond the modulation region of single soliton microcomb. The result paves the way for developing all-solid-state and ultrahigh-frame-rate coherent LiDAR systems.

Recently, the light detection and ranging (LiDAR) system is emerging for the development of the artificial intelligence (AI), such as autonomous driving, unmanned aerial vehicle and so on. The advanced AI application has the demand of massive data stream and fast processing capability[1,2].

The parallel laser ranging has been reported with the massively individual laser diode array on flash or mechanical LiDAR[3,4]. The tens or hundreds of lasers greatly increase the cost and assembly difficulty. Microcombs, pumped by only one laser, have been utilized to obtain tens of distinct channel for parallel sensing[5–7]. In one direction, these distinct channels can be mapped to the pixels through a diffraction optics, such as volume gratings. But beam scanning in the orthogonal direction, all of them, is performed through a mirror galvanometer as the traditional mechanical LiDAR. Thus, the robustness and integration level need to be improved further.

The all-solid-state and miniatured LiDAR is the trend for the parallel operation. Inertialess beam steering based on silicon integrated optical phased array (OPA) is an essential component for the solid-state LiDAR. High performance integrated OPA should have a wide field of view and a small beam divergence. In the reported one-dimensional (1D) OPA, phase tuning combining with wavelength tuning is utilized for two-dimensional (2D) beam steering. For the horizontal direction, beam steering of a large field of view (FOV) can be realized by the antenna arrangement of sparse[8–10] or half-wavelength period[11,12], in which the phase error is corresponding to the beam quality. The OPA with four beams, carrying different phase information, has been reported for the parallel scanning based on Butler matrix[13], which is difficult to demodulate receiving signal and scale up the array. For the vertical direction, the beam steering could be realized by wavelength tuning based on tunable lasers[14,15]. However, multiple individual tunable lasers would be required for parallel

[1]State Key Laboratory for Extreme Photonics and Instrumentation, International Research Center for Advanced Photonics, Ningbo Innovation Center, College of Optical Science and Engineering, Zhejiang University, Hangzhou 310058, China. [2]National Key Laboratory of Microwave Photonics, College of Electronic and Information Engineering, Nanjing University of Aeronautics and Astronautics, Nanjing 211016, China. [3]Photonics Research Institute, Department of Electrical and Electronic Engineering, The Hong Kong Polytechnic University, Kowloon, Hong Kong SAR, China. [4]These authors contributed equally: Jingye Chen, Wenlei Li, Zhe Kang. e-mail: yaocheng@zju.edu.cn

wavelength scanning. The beam divergence and multi beams quality are challenging and essential performances for realizing the parallel beams emission, carrying distinct wavelength information. The ultra-long optical grating antenna with a low coupling constant and a low phase error is usually required for a small divergence. The millimeter-scale antenna can be realized by small etching corrugations of silicon waveguide[16] or assisted with the multi-layer material such as silicon nitride[17,18]. However, it demands a high lithography precision, etching precision, or heterogeneous material growth, which has a high fabrication complexity and high cost.

In the detection terminal, the coherent method is usually superior to the other implementations in the circumstance of low-visibility or high-background-light. Since the theoretical sensitivity of coherent detection can be up to the quantum noise limit[19]. At the same time, the on chip OPA combining with the frequency-modulated continuous-wave (FMCW) method is recognized as the best alternatives for realizing a miniature coherent LiDAR in the future.

In this work, we proposed and experimentally demonstrated an integrated OPA combined with microcomb. The OPA is based on a 1D sparse arrangement of optical antenna array, having a large FOV without grating lobes in the horizontal direction. There is also a small beam divergence in the vertical direction, which is harnessing the bound state in the continuum (BIC) effect on silicon waveguide grating antenna. To achieve a high beam quality, the wide waveguide beyond single mode region is adopted for the OPA. The measured beam divergence is about 0.037° with the long optical grating antenna, which is consistent with the comb tooth spacing (101.3 GHz) and optical beam of Rayleigh criterion. The multiple comb tooth, carrying distinct wavelength information, are output and steered by the integrated OPA. The all-solid-state parallel LiDAR has been demonstrated with the FMCW method for three-dimensional (3D) ranging. External modulation is utilized to obtain the parallel frequency modulated multi-wavelength laser source with only one pump laser. The distance deviation is measured to be about 2.5 cm at meter scale range.

Figure 1 shows the schematic of the proposed microcomb combined with integrated OPA for parallel LiDAR, which consists of a continuous wave (CW) pump laser, microcomb, electro-optical modulator (EOM), OPA chip, and coherent detection array. The microcomb chip, generating multiple comb tooth, is based on the silicon nitride platform and pumped by the single CW laser. The multiple comb frequencies are parallelly modulated by the EOM for generating FMCW signal. The OPA chip is based on commonly used the silicon-on-insulator (SOI) platform with a 220 nm-thick silicon core layer. The OPA consists of a power splitter tree, a voltage-controlled phase shifter array, and an optical antenna array. The input light is uniformly split into different channels of phase shifters. The thermo-optics phase shifters are tuned by a multi-channel voltage controller. The waveguides are then fanned out to the sparse antenna array. The long optical antenna, harnessing BIC effect, has small beam divergence in the vertical direction. Principally, we utilize phase tuning combining with wavelength tuning for two-dimensional (2D) beam steering. For the horizontal direction (phased array direction), beam steering is realized by phase tuning with independently voltage-controlled phase shifter elements. For the vertical direction (comb direction), the parallel beam scanning can be realized by multiple wavelengths of the optical comb. The multiple comb tooth, carrying distinct wavelength information, are output and steered by the integrated OPA, which is without mechanical modules for two-dimensional beam scanning. The frequency mixing of echo signal (ES) and local oscillator (LO) is developed and the beat signals are output to the processor, namely FMCW coherent detection.

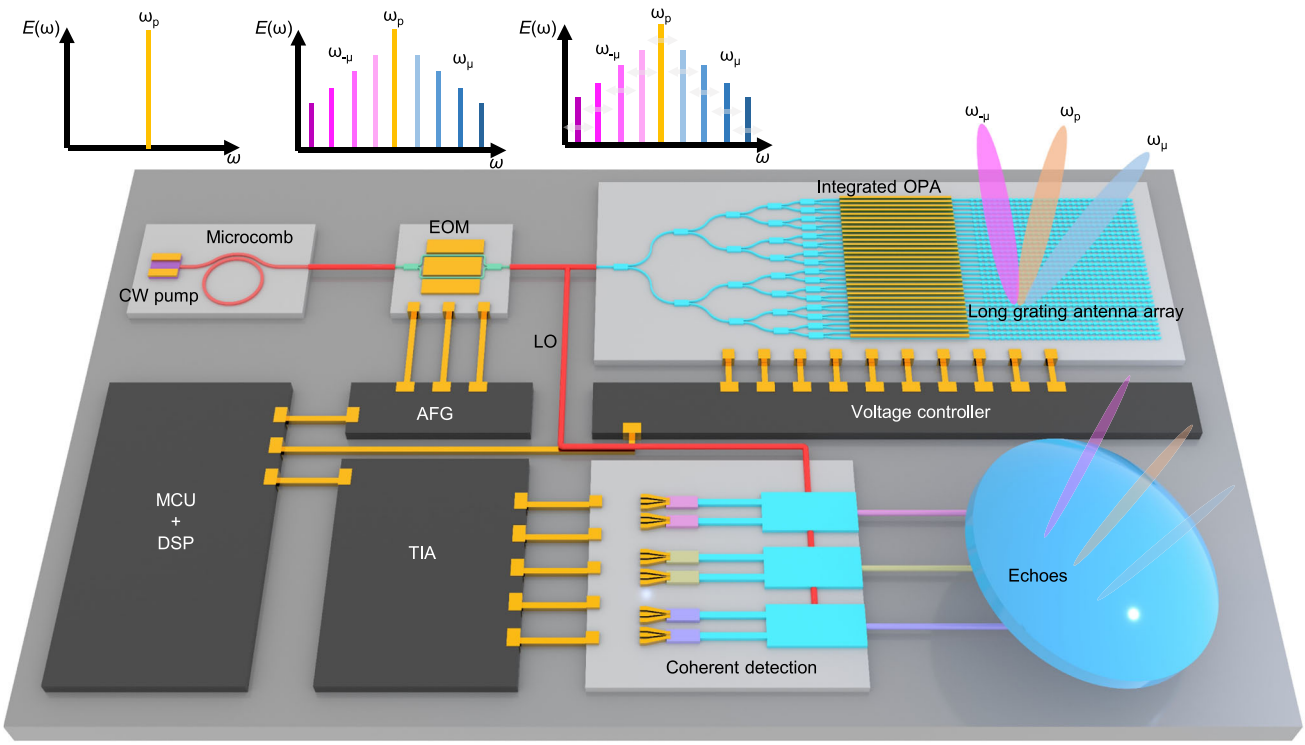

Fig. 1 | Parallel FMCW LiDAR system. Conceptual illustration of FMCW system based on integrated microcomb combined with OPA. The comb is pumped by the CW laser. The multiple comb frequencies are externally modulated by the EOM and beam steering is operated by the integrated OPA. The multiple echoes are received by coherent detection based on wavelength multiplexing to obtain the information of distance and velocity of targets. OPA optical phased array, CW continuous wave, EOM electro-optical modulator, AFG arbitrary function generator, LO local oscillator, TIA transimpedance amplifier, MCU microcontroller unit, DSP digital signal processor.

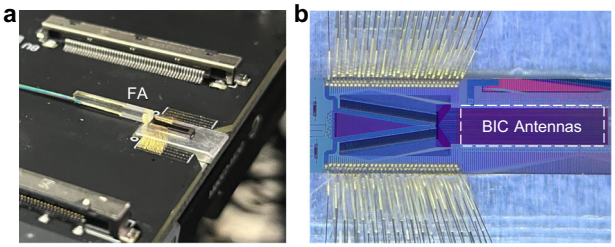

Fig. 2 | Optical microscopy images. a The packaged chip, and (**b**) the fabricated OPA chip. FA fiber array, BIC bound state in the continuum.

Results

Single soliton microcomb generation

A single soliton microcomb contributes to the parallel and coherent CW sources of the proposed integrated solid-state FMCW LiDAR. Supplementary Fig. S1(a) shows the microscope image of the characterization of microring resonators. The microring utilized in the experiments has a radius of 229 μm, corresponding to the FSR of 101.3 GHz. The temperature of the soliton microcomb chip is controlled by a thermo-electric cooler (TEC). Generation of the single soliton microcomb in the experiment is probabilistic. Deterministic generation of single soliton microcomb can be assisted by several methods reported, such as optical cooling of a blue-detuned auxiliary light provided by either an independent continuous wave laser[20,21] or a modulated pump sideband[22], a self-injection locking[23], a trigger pulse[24], and so on. Supplementary Fig. S1b shows the experimental setup of the soliton microcomb generation and measurement. The pump to comb conversion efficiency is about 1.53%. Supplementary Fig. S1c shows the spectral profiles of the modulation instability (MI), chaos, two-soliton, and single-soliton microcombs, respectively, during the pump scanning process. To implement the parallel CW sources for the OPA chip, twenty comb teeth are selected with power differences of <3 dB. The extinction ratio of the comb teeth is about 15 dB, which can be increased to >40 dB by filtering the noise of the pump light.

Beam steering operated by OPA

The OPA consists of a power splitter tree, a voltage-controlled phase shifter array, and an optical antenna array. For the horizontal direction (phased array direction), beam steering is realized by phase tuning with independently voltage-controlled phase shifter elements. For the vertical direction (comb direction), the parallel beam scanning can be realized by multiple wavelengths of the optical comb. Principally, according to the Rayleigh criterion, the small beam divergence in the vertical direction is required to separate the adjacent wavelength channels of the microcomb. First, the beam divergence is defined by the effective length of antenna. Larger effective length of antenna, smaller beam divergence. Second, the effective length of antenna is related to the diffraction strength α. Weaker diffraction strength, larger effective length of antenna (Supplementary Note 1). Thus, the millimeter-long grating antenna is one of the key components for separating the adjacent wavelength channels of the microcomb in the free space. Diffraction strength of a grating antenna is correlated with the effective refractive index perturbation of the waveguide structure[25]. Conventionally, the small etching corrugation or low refractive index material such as silicon nitride is used to achieve weak diffraction strength. However, such methods are challenging in terms of process complexity as well as fabrication precision. The hybrid platform requires additional material deposition and several etching steps, leading to the relatively complex fabrication process compared with the single step etching of single layer of silicon. Furthermore, the conventional small etching corrugation will cause relatively large lateral radiation, in which the theoretical antenna length will be limited by the unnecessary radiation loss.

Here, we utilize the side-etched grating antenna with periodic rectangular nanogrooves on both sides of the waveguide, as shown in Supplementary Fig. S2a. The propagation mode (TE_0) of the grating antenna can be coupled to the radiation modes through the nanogrooves, where the lateral radiation modes have an equivalent path difference with the width of the waveguide. And the diffraction strength of the grating antenna can be dramatically reduced by manipulating the width of the waveguide to build a destructive interference between the lateral radiation modes, known as the quasi-bound state in the continuum (qBIC)[26]. The device is designed based on the SOI platform with a 220 nm core silicon thickness, and the edge length d_{grt} of the rectangular nanogrooves is selected to be 180 nm in order to meet the feature size of the fabrication process. The grating pitch Λ_{grt} is chosen to be 600 nm with the corresponding steering angle θ of about 10.4° at the 1550 nm wavelength. The diffraction strength α of the grating antenna is calculated for different waveguide width W_{grt}, as shown in Supplementary Fig. S2b. It can be found that α periodically reaches the minimum value, corresponding to the different order of qBIC. Here, the waveguide width W_{grt} is selected as 1.02 μm for the second-order qBIC ($qBIC_2$), which is beyond the single mode region, for lower perturbation of the corrugation. The diffraction strength of the grating antenna is <0.015 dB/μm, and the antenna with a length of 1.3 mm can theoretically achieve a far-field beam divergence of 0.05°.

The power consumption of phase shifter is measured to be 18.5 mW/π for TE polarization by measuring the fabricated Mach-Zehnder interferometer (MZI) structures. The excess loss of 3-dB power splitter based on multi-mode interferometer (MMI) is 0.12 dB. The optical antenna element, one of the key devices, is also characterized. To directly demonstrate the $qBIC_2$ effect of the antenna, we measure the diffraction strength for the fabricated grating antennas. A series of antennas with varied l_{grt} (from 200–2000 μm) are fabricated to evaluate diffraction strength α. The straight waveguides without nanogrooves are also fabricated on the same chip for power normalization. As shown in Supplementary Fig. S3, the diffraction strength α, induced from the normalized transmission various with antenna length, is about 0.00685 dB/μm. The diffraction strength is relatively smaller than the calculated ones, due to the fabrication error induced. The depth d_{grt} is shrunk to be about 140 nm in the fabrication process.

To verify the proposed strategy, we fabricate a 128-channel OPA chip, integrating the couplers, the phase shifters, optical grating antennas, and so on. Deep trenches between adjacent phase shifters are used to reduce the thermal crosstalk during modulation, and the waveguide lengths for each channel of the OPA are equalized to eliminate wavelength dependence in beamforming. Figure 2a, b show the optical microscope images of the OPA chip as well as the opto-electronic packaging, respectively.

To break the limitation of the grating lobes in horizontal direction φ, the sparse method is utilized in the 1D antenna array. With the sparse antenna array arrangement, there is only one main beam in the FOV. After the phase calibration with a genetic algorithm, the beam is well calibrated at 0°. As shown in Supplementary Fig. S4, the full width at half-maximum (FWHM) is of 0.1° in the horizontal direction φ and 0.037° in the vertical direction θ, respectively, with a high sidelobe suppression. The smaller the diffraction strength α, the longer optical grating antenna, which will extend the effective aperture. Thus, the measured beam divergence is smaller than the calculated one. The beam divergence can be further reduced by increasing the number of antenna element and reducing the grating corrugation. Here, for parallel beam scanning with different wavelengths, the beam divergence of 0.037° in vertical direction θ can satisfy the Rayleigh criterion with a comb tooth spacing of 101.3 GHz.

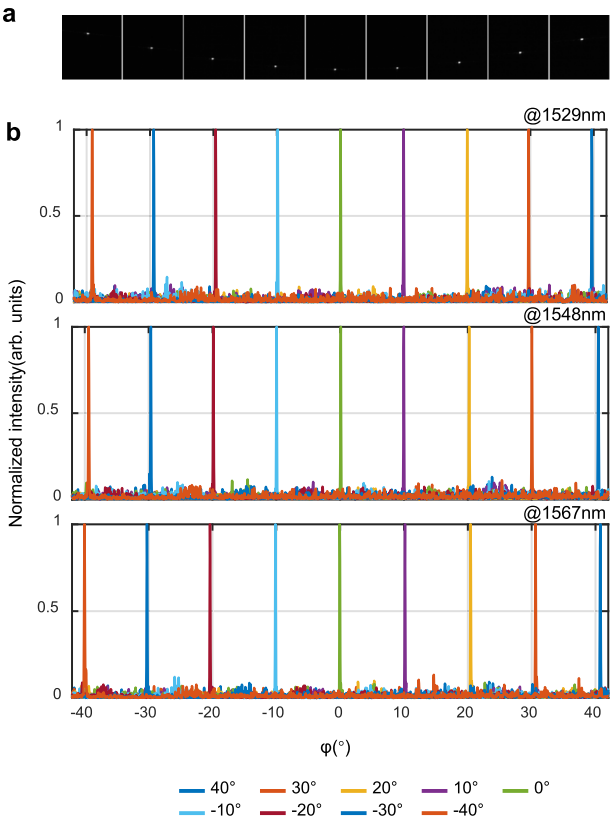

Fig. 3 | The measured beam performance in horizontal direction. a The spliced image of far-field beam after calibration at different steered angles at one typical wavelength. **b** The measured far-field intensity distribution in horizontal direction at three typical wavelengths of 1529 nm, 1548 nm, and 1567 nm.

We characterize the beam steering in vertical direction with the wavelength ranging from 1529–1567 nm, which is around the pump wavelength of microcomb (Supplementary Note 2). Supplementary Fig. S5a shows the measured far-field image at different wavelengths. And the normalized far-field beam intensity distribution curves along the vertical direction are shown in Supplementary Fig. S5b. The beam steering range is about 5° within the 38 nm wavelength band. The wavelength tuning efficiency is measured to be $|\kappa| = 0.138°/\text{nm}$ by using the linear fitting method, as shown in Supplementary Fig. S5c. The beam steering range is usually limited by the wavelength tuning range of the light source and the bandwidth of passive devices, such as power splitters and grating antennas (Supplementary Note 3). To solve this problem, two approaches have been reported, of which one is the multi-line OPA[27,28] and another is the multidimensional multiplexing OPA[15,29,30]. The total steering angle and the wavelength tuning efficiency can be up to twice of conventional ones with the same tuning wavelength band.

In horizontal direction, Fig. 3a shows the image of the normalized far-field main beam at ±40°, ±30°, ±20°, ±10°, and 0°, respectively, under the laser wavelength of 1548 nm. The measured image resolution and FOV of the OPA chip is limited by the optical imaging system, such as the numerical aperture (NA) of lens and the size and number of charge-coupled device (CCD) pixel, which has a trade-off. The normalized far-field distributions in the horizontal direction at three typical wavelengths (1529, 1548, and 1567 nm), are shown in Fig. 3b. With the same voltage series of phase control, the far field beams at different wavelengths are all with high beam quality and high sidelobe suppression ratio of >8 dB, which is contributed to the large number and the sparse distribution of antennas. To illustrate the high performance 2D beam scanning without mechanical rotation, the OPA scanner is utilized to develop the character patterns of "Z", "J", and "U", which is tuned with wavelength step of 0.8 nm in vertical direction and the angle step of 0.2° in horizontal direction, as shown in Supplementary Fig. S6.

When the high performance OPA chip combined with the microcomb, the massively parallel beam steering in 2D area can be realized. As a prototype verification, the tens of beams, simultaneously transmitted in vertical direction, can be utilized for parallel scanning. The output soliton microcomb is filtered by a fiber Bragg grating (FBG) notch filter to decrease the pump residue, as shown in Fig. 4a. Figure 4b shows the parallel beam scanning in the vertical direction at nine discrete horizontal angles, representatively. Actually, the parallel beams can be continuously steered with continuous phase tuning by the OPA. The angle of parallel beams is slightly oblique in the photos of camera, due to the mapping of spherical coordinates to cartesian coordinates.

Characterization of parallel FMCW lidar

As a prototype, we also characterize the ranging performance of the microcomb combined with OPA for the FMCW detection. The external modulation method is used to generate the frequency modulation signal. Supplementary Fig. S7a shows the schematic setup of the parallel FMCW LiDAR. The amplified continuous wave laser is utilized as the pump laser of the microcomb. The narrow band filter is used to decrease the pump wavelength at the output of microcomb. Supplementary Fig. S7b shows the typical spectra of the microcomb before and after modulation by the SSB. It can be found that all the comb teeth simultaneously generate a sideband signal with a frequency shift same as the RF signal. The frequency modulation nonlinearities of the comb lines are $<1.77 \times 10^{-7}$ (Supplementary Note 6). The power of the comb lines varies randomly of about 2 dB because of the amplified spontaneous emission (ASE) noise. The comb line at long wavelength is about 10 dB higher than the short wavelength, since the soliton comb spectrum (excluding the pump) is red-shifted due to the dispersive-wave-recoil and Raman induced soliton self-frequency shift[31]. Compared to modulating the pump laser for achieving linear frequency modulation continuous wave, the parallel modulation of the output microcomb is helpful to maintain the stability of the single soliton state, not perturbing the repetition rate and power, and the linear modulation bandwidth is beyond the modulation region of single soliton microcomb. Though the number of simultaneously modulated comb lines will be limited by the optical bandwidth of the external modulator (usually ~40 nm), ~50 comb lines can dramatically increase the frame rate of point cloud.

Limited by the receiving aperture of the collimator, a tunable band-pass filter (TBPF) is used to sequentially select individual comb tooth for distance detection of the target. With the lower optical chip loss and higher sensitivity photodetector, the source power can be dramatically decreased. Thus, it is practical for much more comb lines working at the same time with silicon nitride waveguides and higher performance of OPA chips and detectors. It should be noted that the microcomb is spectral channel separated and the analysis of the beat signal is also operated in the frequency domain. Since the temporal sequential detection does not affect the frequency information, this experimental method can be considered as an equivalent demonstration of parallel ranging. The strict coaxial transceiver based on single OPA structure can also be introduced to the all-solid-state transceiving LiDAR system[32].

Figure 5a, b show the images of the far-field beam of the 1550.27 and 1551.1 nm wavelength channel, respectively, and the corresponding beat signal spectra are shown in Fig. 5c. It can be found that the beat signals of the two adjacent channels have different peak frequencies, indicating that the far field beam of the adjacent channels are distinguishable.

https://doi.org/10.1038/s41467-025-56483-9

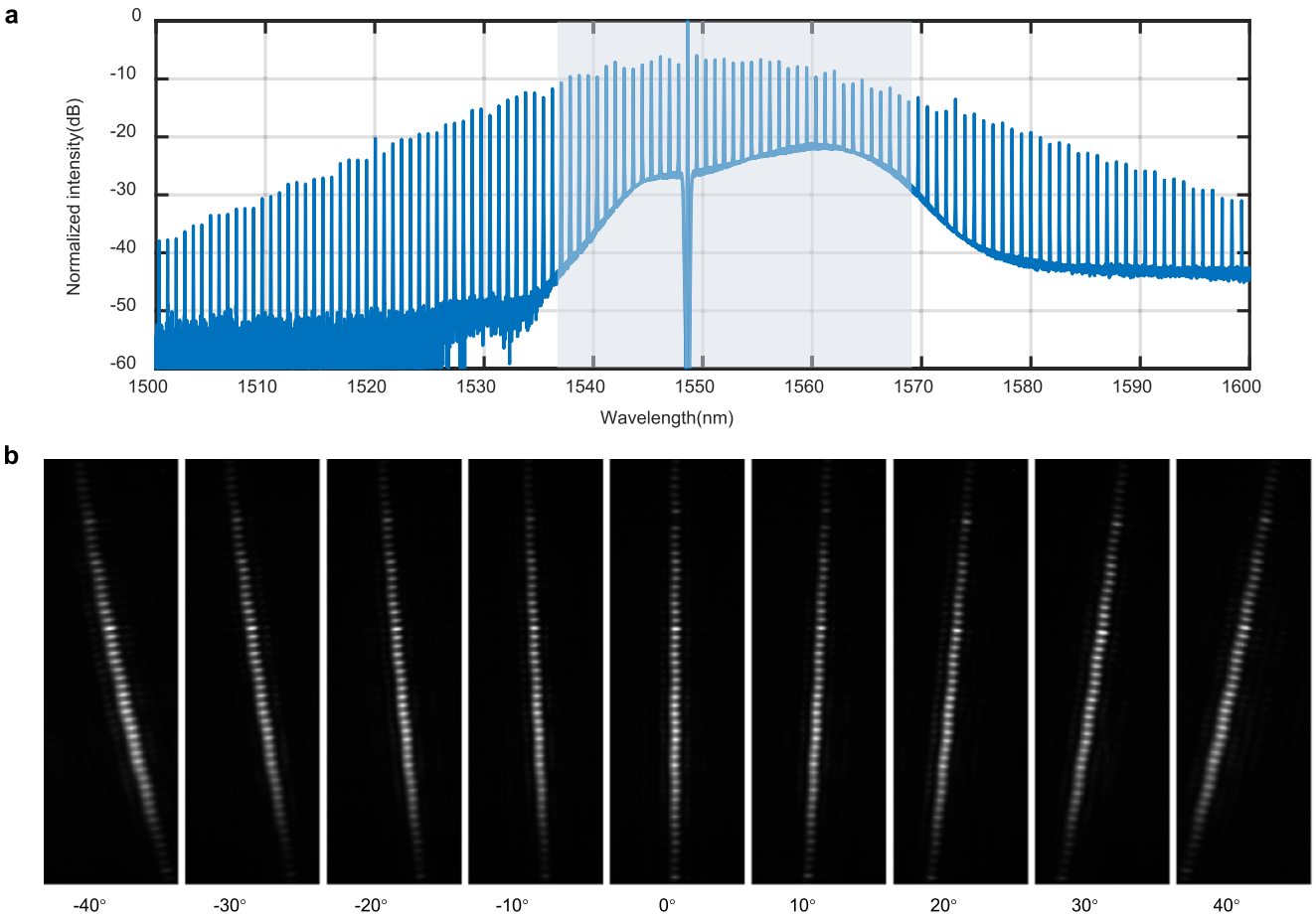

Fig. 4 | Characterization of parallel beam scanning. a Spectra of the microcomb after notch filter. The shaded area highlights the comb lines used for parallel scanning. **b** The far-field images after calibration for the far-field beam at ±40°, ±30°, ±20°, ±10°, and 0° with light source of the single soliton comb.

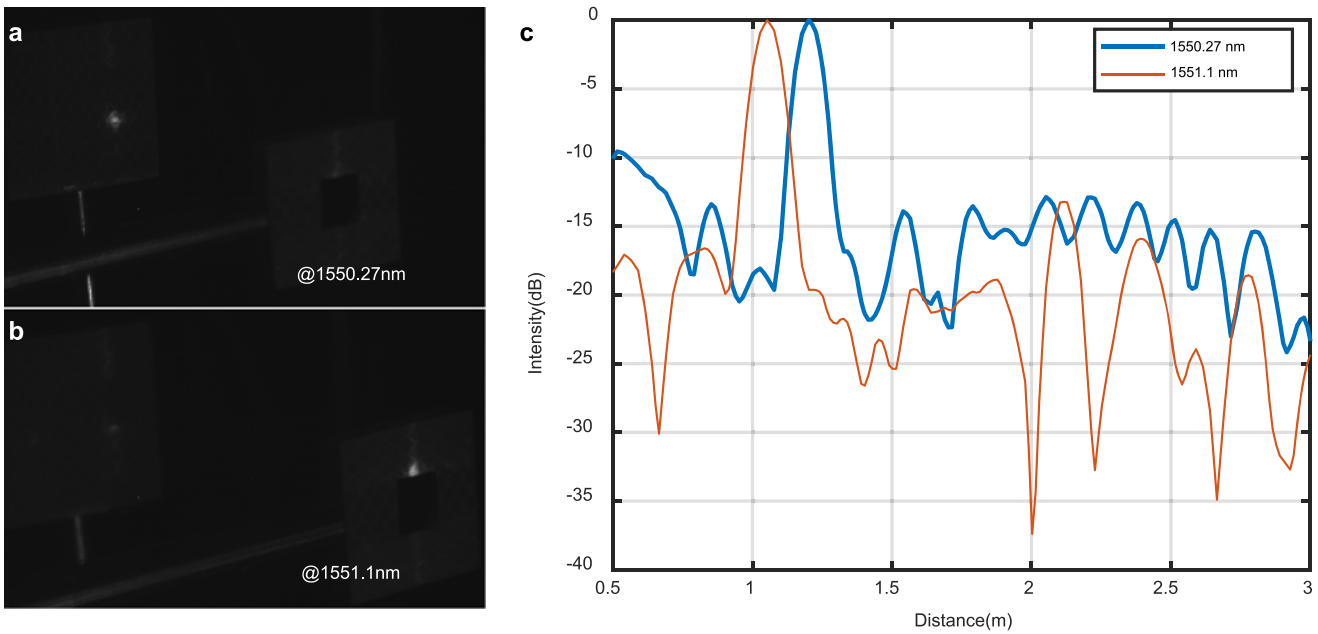

Fig. 5 | Far field beams of two adjacent wavelength channels. Far-field beams of wavelength channels at (**a**) 1550.27 nm and (**b**) 1551.1 nm. **c** Beat signal spectra of the two adjacent wavelength channels.

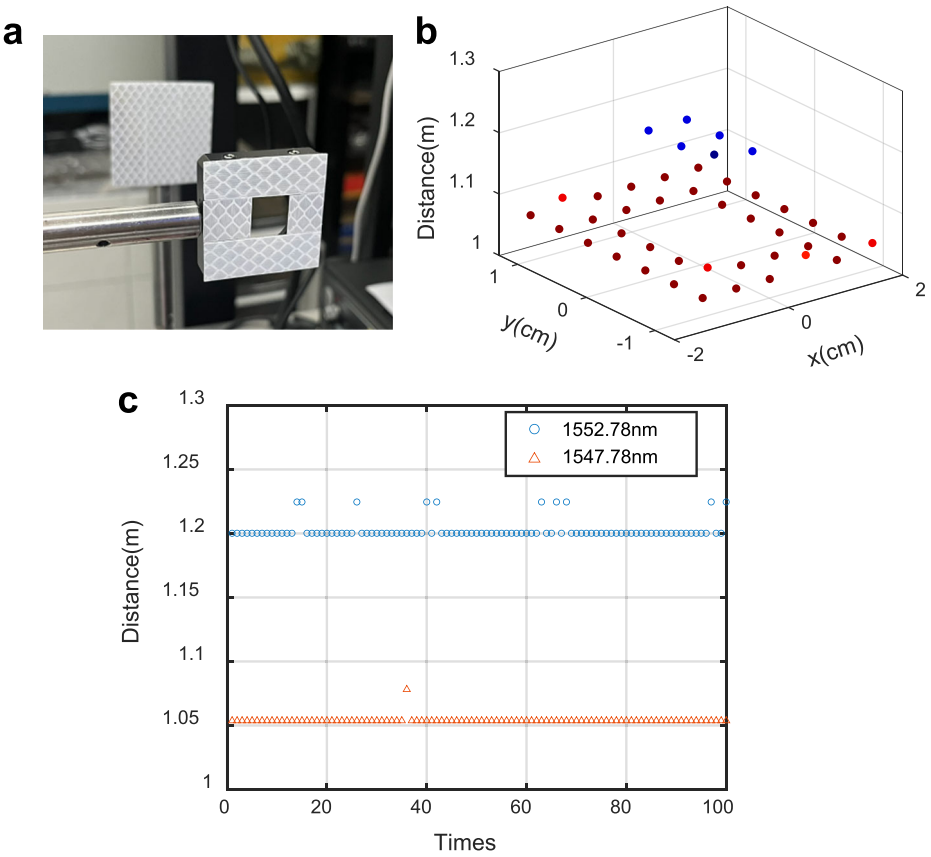

Fig. 6 | 3D LiDAR imaging. a Picture of the target objects. **b** The measured 3D point cloud image. **c** The object distances obtained from 100 continuous measurements, showing good consistency.

3D LiDAR imaging is then demonstrated by combining beam steering in the phase direction. As shown in Fig. 6a, the reflective targets are two vertically placed reflective cardboards, of which the forward one has a rectangular hole in the center. The two cardboards spaced by 15 cm are placed at a distance of about 1.1 m away from the OPA chip. Considering the flatness of the comb lines, a set of data are measured at a step of two microcomb teeth, and a total of seven wavelength channels are selected as a proof of concept, as shown in Supplementary Fig. S7b. The commercial waveshaper or the on-chip multichannel amplitude equalizer[33] could be used further to flatten out the comb spectrum. In the phase direction, the angle step is 0.32° and six angle positions are selected. Figure 6b shows the measured 3D point cloud image of the targets (Supplementary Note 7).

Finally, the distance measurement stability is characterized. As an example, two wavelength channels of 1552.78 nm and 1547.78 nm are selected to measure the distance of the target object for 100 consecutive times, and the measured results are shown in Fig. 6c. It can be found that the ranging results have a good consistency. There are a few measurements showing a distance deviation of 2.5 cm, which is mainly due to the low signal-to-noise ratio (SNR) of the beat signal and can be further improved by increasing the received signal power and higher performance of commercial detectors.

Discussion

In summary, we propose and demonstrate an integrated OPA combined with single soliton microcomb. The 1D OPA with a millimeter-long grating antenna is utilized for the 2D steering. The antenna is based on the BIC effect and with only one-step fully etching to ease the fabrication. The low phase error enables the multiple optical beams, carrying different wavelength information, to transmit simultaneously. The experimental results indicate that the beam divergence in the vertical direction is ~0.037°, and the FOV is 80° without grating lobes in the horizontal direction. In the vertical direction, the OPA, combined with single soliton microcomb, can be utilized for tens of parallel beam scanning. The different soliton comb states, e.g. soliton crystals, multi-solitons, and single soliton, can all be used for the coherent LiDAR application in future. Thus, the variable beam lines can be obtained for different strategies of beam scanning for region of interest. The parallel LiDAR system is demonstrated with FMCW ranging, which can dramatically increase the frame-rate. The drawback of the architecture is that it requires a balanced photodetector array and a wavelength-division demultiplexer array. However, the integration of demultiplexers is straightforward via arrayed waveguide gratings and chip-scale integration of large banks of balanced photodetectors has been recently demonstrated, having the potential to be utilized in the parallel LiDAR system.

The destination of the solid-state LiDAR is to develop a fully integrated system. The system can integrate the soliton microcomb generator driven by an on-chip laser, filters, the transceiving OPA, modulators, photodetectors, and so on[34]. Hybrid or heterogeneous integrated microcombs with on-chip lasers have been studied and experimentally demonstrated as compelling solutions[23,35,36]. The key challenge is the power budget of the LiDAR system. The on-waveguide powers of both approaches of fully integrated comb source are limited to tens of milliwatts. An alternative is to increase the conversion efficiency of soliton microcomb generation by resonance-shifted coupled-microresonators[37]. The erbium-doped waveguide amplifier (EDWA), fabricated by erbium ion implantation into an ultra-low loss silicon nitride photonic integrated circuit, is also a promising way to overcome the power budget problem of the integrated chip[38]. Such excellent on-chip high power performance is promising for realizing the fully integrated LiDAR system. We believe that the proposed

scheme is promising of full integration for all-solid-state and miniature LiDAR system, such as autonomous driving and unmanned aerial vehicle, which are demanding the high-speed 3D sensing.

Methods

Fabrication of microcomb and OPA chip

The soliton microcomb is generated in the high Q-factor silicon nitride (Si_3N_4) microring resonators which are fabricated by the standard AN800 multi-project wafer run (Ligentec, Switzerland).

The proposed OPA chip is fabricated on the 220 nm SOI platform with the lithography followed by the inductively coupled plasma reactive ion etching (ICP-RIE) process. The heater material is titanium nitride. The chip is also packaged with a fiber array and wire-boned with a printed circuit board (PCB) for external voltage control. The insertion loss of the edge coupler is 2.1 dB/facet.

Experimental details

A CW tunable laser (Toptica Photonics CTL 1550) serves as the pump source to continuously drive the microring. The power of the pump light is boosted to 500 mW by an erbium-doped fiber amplifier (EDFA). To generate the single soliton microcomb, the pump laser is scanned from the blue-detuned side to the effective red-detuned side of the cavity resonance. The TEC is simultaneously adjusted to control the temperature of the soliton microcomb chip. The spectra of the microcombs are measured by an optical spectrum analyzer (Yokogawa AQ6370D). The $sech^2$ fitting curves confirm the two-soliton and single soliton signature of the microcombs.

The amplified spontaneous emission (ASE, B&A) source, optical spectrum analyzer (OSA, Yokogawa AQ6370D), and sourcemeter are used to characterize the performance of the fabricated key devices, such as phase shifters and long grating antennas.

The arbitrary waveform generator (AWG) and the single-sideband modulator (SSB) are utilized to generate the linear triangular wave signal. The AWG (Keysight 8195 A) generates a triangularly modulated sinusoidal radio frequency (RF) signal to drive the SSB (Fujitsu FTM7962EP) with a carrier frequency of 13 GHz. The linear frequency modulation bandwidth is 3 GHz, and the waveform period is set to be 10 μs.

The filtered soliton microcomb is re-boosted to 40 mW by the EDFA, delivered as an example, and split into two branches by a 10:90 optical power splitter. One branch serves as the LO source for coherent detection. Another branch is launched into the OPA chip for scanning. The echo signal is received by a collimator (Thorlabs, F810APC-1550) and hybridized with the LO to form a beat signal, which is detected and recorded by a balanced photodetector (KY-BPRM-XX-I-FA) and oscilloscope (Keysight, DSO7032B).

Data availability

The data that support the findings of this study are available from the corresponding authors upon request. Source data are provided with this paper.

References

1. Feldmann, J. et al. "Parallel convolutional processing using an integrated photonic tensor core,". *Nature* **589**, 52–58 (2021).
2. Asakawa, K., Sugimoto, Y. & Nakamura, S. Silicon photonics for telecom and data-com applications. *Opto Electron. Adv.* **3**, 200011 (2020).
3. Zoysa, M. et al. Non-mechanical three-dimensional LiDAR system based on flash and beam-scanning dually modulated photonic crystal lasers. *Optica* **10**, 264–268 (2023).
4. Alsadik, B. Ideal angular orientation of selected 64-channel multi beam lidars for mobile mapping systems. *Remote Sens.* **12**, 510 (2020).
5. Riemensberger, J. et al. Massively parallel coherent laser ranging using a soliton microcomb. *Nature* **581**, 164–170 (2019).
6. Lukashchuk, A., Johann, R., Aleksandr, T., Liu, J. & Kippenberg, T. J. Chaotic microcomb-based parallel ranging. *Nat. Photonics* **17**, 814–821 (2023).
7. Chen, R. et al. Breaking the temporal and frequency congestion of LiDAR by parallel chaos. *Nat. Photonics* **17**, 306–314 (2023).
8. Komljenovic, T., Helkey, R., Coldren, L. & Bowers, J. E. Sparse aperiodic arrays for optical beam forming and LIDAR. *Opt. Express* **25**, 2511–2528 (2017).
9. Hutchison, D. N. et al. High-resolution aliasing-free optical beam steering. *Optica* **3**, 887–890 (2016).
10. Li, W. et al. High-speed 2D beam steering with large field of view based on thin-film lithium niobate optical phased array. *Photonics Res.* **11**, 1912–1918 (2023).
11. Phare, C. T., Shin, M. C., Miller, S. A., Stern, B. & Lipson, M. "Silicon optical phased array with grating lobe-free beam formation over 180 degree field of view,". *arXiv* https://doi.org/10.1364/CLEO_SI.2018.SM3I.2 (2018).
12. Liu, Y. & Hu, H. Silicon optical phased array with a 180-degree field of view for 2D optical beam steering. *Optica* **9**, 903–907 (2022).
13. Lu, P. et al. Integrated multi-beam optical phased array based on a 4 × 4 Butler matrix. *Opt. Lett.* **46**, 1566–1569 (2021).
14. Li, Y. et al. Wide-steering-angle high-resolution optical phased array. *Photonics Res.* **9**, 2511–2518 (2021).
15. Zhao, S., Lian, D., Chen, J., Dai, D. & Shi, Y. Polarization multiplexing silicon photonic optical phased array with a wide scanning range. *Opt. Lett.* **48**, 6092–6095 (2023).
16. Miller, S. A. et al. *"512-Element Actively Steered Silicon Phased Array for Low-Power LIDAR,"*. https://opg.optica.org/abstract.cfm?uri=cleo_si-2018-JTh5C.2 (2018).
17. Xu, W. et al. Fully integrated solid-state LiDAR transmitter on a multi-layer silicon-nitride-on-silicon photonic platform. *J. Lightwave Technol.* **41**, 832–840 (2023).
18. Raval, M., Poulton, C. V. & Watts, M. R. Unidirectional waveguide grating antennas with uniform emission for optical phased arrays. *Opt. Lett.* **42**, 2563–2566 (2017).
19. Poulton, C. V. et al. Coherent solid-state LIDAR with silicon photonic optical phased arrays. *Opt. Lett.* **42**, 4091–4094 (2017).
20. Zhou, H. et al. Soliton bursts and deterministic dissipative Kerr soliton generation in auxiliary-assisted microcavities. *Light Sci. Appl.* **8**, 50 (2019).
21. Zhang, S. et al. Sub-milliwatt-level microresonator solitons with extended access range using an auxiliary laser. *Optica* **6**, 206–212 (2019).
22. Wildi, T., Brasch, V., Liu, J., Kippenberg, T. J. & Herr, T. Thermally stable access to microresonator solitons via slow pump modulation. *Opt. Lett.* **44**, 4447–4450 (2019).
23. Shen, B. et al. Integrated turnkey soliton microcombs. *Nature* **582**, 365–369 (2020).
24. Kang, Z. et al. Deterministic generation of single soliton Kerr frequency comb in microresonators by a single shot pulsed trigger. *Opt. Express* **26**, 18563–18577 (2018).
25. Shang, K. et al. Uniform emission, constant wavevector silicon grating surface emitter for beam steering with ultra-sharp instantaneous field-of-view. *Opt. Express* **25**, 19655–19661 (2017).
26. Xu, H. & Shi, Y. Diffraction engineering for silicon waveguide grating antenna by harnessing bound state in the continuum. *Nanophotonics* **9**, 1439–1446 (2020).
27. Tyler, N. A. et al. SiN integrated optical phased arrays for two-dimensional beam steering at a single near-infrared wavelength. *Opt. Express* **27**, 5851–5858 (2019).
28. Zhang, L. et al. Large-scale integrated multi-lines optical phased array chip. *IEEE Photonics J.* **12**, 6601208 (2020).
29. Han, X. et al. Solid-state photonics-based Lidar with large beam-steering angle by seamlessly merging two orthogonally polarized beams. *IEEE J. Sel. Top. Quant. Electron.* **27**, 8300608 (2021).

30. Zhao, S., Chen, J. & Shi, Y. Dual polarization and bi-directional silicon-photonic optical phased array with large scanning range. *IEEE Photonics J.* **14**, 6620905 (2022).
31. Yi, X. et al. Single-mode dispersive waves and soliton microcomb dynamics. *Nat. Commun.* **8**, 14869 (2017).
32. Chen, J. et al. Coaxial transceiving LiDAR based on a silicon photonic optical phased array. *Opt. Lett.* **49**, 3424–3427 (2024).
33. Zhang, C. et al. Reconfigurable multichannel amplitude equalizer based on cascaded silicon photonic microrings. *Photon. Res.* **11**, 742–749 (2023).
34. Kim, I. et al. Nanophotonics for light detection and ranging technology. *Nat. Nanotechnol.* **16**, 508–524 (2021).
35. Chang, L., Liu, S. & Bowers, J. E. Integrated optical frequency comb technologies. *Nat. Photon.* **16**, 95–108 (2022).
36. Ji, Q. et al. Engineered zero-dispersion microcombs using CMOS-ready photonics. *Optica* **10**, 279–285 (2023).
37. Helgason, Ó. B. et al. Surpassing the nonlinear conversion efficiency of soliton microcombs. *Nat. Photon.* **17**, 992–999 (2023).
38. Liu, Y. et al. A photonic integrated circuit–based erbium-doped amplifier. *Science* **376**, 1309–1313 (2022).

Acknowledgements

Y. S. acknowledges the funding from the National Major Research and Development Program (2021YFB2801703), the National Natural Science Foundation of China (62135011), the "Pioneer" and "Leading Goose" R&D Program of Zhejiang (2022C01103), the Leading Innovative and Entrepreneur Team Introduction Program of Zhejiang (2021R01001), and the Fundamental Research Funds for the Central Universities. J.C. acknowledges the funding from National Natural Science Foundation of China (62105286). Z.K. acknowledges the funding from National Natural Science Foundation of China (62075188).

Author contributions

All authors contributed extensively to the work presented in this paper. Y.S. conceived the study. J.C., W.L, D.D., and Y.S. designed and characterized the OPA chip. Z.L., Z.K., J.H., and D.H. designed and characterized the comb chip. J. C., W. L., S.Z., and D. L. performed the system measurements. All authors participated in data analysis and discussion. J.C., W.L., Z.L., Z.K., D.D., and Y.S. conducted theoretical analysis. J.C., W.L., Z.K., and Y.S., wrote the manuscript with input from all coauthors. Y.S. supervised the research.

Competing interests

The authors declare no competing interests.

Additional information

Supplementary information The online version contains supplementary material available at https://doi.org/10.1038/s41467-025-56483-9.

Correspondence and requests for materials should be addressed to Yaocheng Shi.

Peer review information *Nature Communications* thanks Junsuk Rho and the other, anonymous, reviewer(s) for their contribution to the peer review of this work. A peer review file is available.